frontiers | Frontiers in Earth Science

ORIGINAL RESEARCH
published: 23 June 2022
doi: 10.3389/feart.2022.904064

Ultra-Deep Dolomite Reservoir Quality Classification and its Effect on Acid-Fracturing Based on Natural Fracture Activity Analysis: A Case Study of the Cambrian Subsalt Reservoir in Northern Uplift of Tarim Basin

Guoqing Yin, Hui Zhang, Yi Xin, Wei Zhang, Xingneng Wu, Jingrui Liang and Shujun Lai*

Research Institute of Exploration and Development, Tarim Oilfield Company, PetroChina, Korla, China

OPEN ACCESS

Edited by:
Lei Gong,
Northeast Petroleum University, China

Reviewed by:
Wenlong Ding,
China University of Geosciences, China
Wenya Lyu,
China University of Petroleum, China

***Correspondence:**
Guoqing Yin
yinguoqing-tlm@petrochina.com.cn

Specialty section:
This article was submitted to Structural Geology and Tectonics, a section of the journal Frontiers in Earth Science

Received: *25 March 2022*
Accepted: *09 May 2022*
Published: *23 June 2022*

Citation:
Yin G, Zhang H, Xin Y, Zhang W, Wu X, Liang J and Lai S (2022) Ultra-Deep Dolomite Reservoir Quality Classification and its Effect on Acid-Fracturing Based on Natural Fracture Activity Analysis: A Case Study of the Cambrian Subsalt Reservoir in Northern Uplift of Tarim Basin. Front. Earth Sci. 10:904064. doi: 10.3389/feart.2022.904064

Taking the >8,000 m buried Cambrian subsalt dolomite reservoir in the northern uplift of the Tarim Basin as an example, this study used imaging logging, cores, outcrops, and other data to identify natural fractures and obtain parameters of natural fractures, including strike, azimuth, width, length, and apparent porosity, and clarified the characteristics of natural fractures in the well section. Based on the logging data, wellbore rock mechanics, *in situ* stress, and elastic parameters were established. The analysis of the mechanical characteristics of natural fractures was carried out to find out the shear stress, normal stress, and their ratio of each natural fracture in the reservoir section. Combined with the stress value of each fracture, the quantitative characterization parameter Fractures Geomechanical Activity Index of the mechanical characteristics of natural fractures is established. Combined with the petrophysical parameters of natural fractures, the evaluation model of the quality index of the reservoir containing the natural fractures is established. According to the classification of reservoir quality, combined with the petrophysical properties of the reservoir section, the optimization of the acid-fracturing scheme and injection pressure can be carried out in order to increase the production after acid-fracturing. In this study, the quality of the reservoir with natural fractures is divided into three categories: the Q_{RCF} of a Class I reservoir is 0.6~1, of Class II reservoir is 0.3~0.6, and of Class III reservoir is less than 0.3. The application of Well L1 and other wells shows that there are great differences in the development of natural fractures at different depths of the Cambrian subsalt dolomite reservoir so as to Q_{RCF}. The Class I reservoir is easy for acid-fracturing to achieve high performance. The Class II reservoir needs large-scale acid-fracturing, and the Class III reservoir cannot be acid-fractured under the current methods. The research results provide a reference for the classification of the fracture mechanical activity of an ultra-deep Cambrian subsalt dolomite reservoir and the optimization of acid-fracturing treatment parameters of similar reservoirs.

Keywords: ultra-deep Cambrian subsalt dolomite reservoir, natural fracture activity, reservoir quality classification, northern uplift, acid-fracturing

1 INTRODUCTION

The main hydrocarbon source rocks of the northern Uplift in the Tarim Basin are ancient and lie in ultra-deep formation, which result in complicated exploration and development of the geological conditions of the ultra-deep formation. The Cambrian subsalt dolomite is the first set of reservoir-cap assemblage above the main hydrocarbon source rocks in the Tarim Basin, which forms the conditions of large-scale oil and gas accumulation (Yang et al., 2020). The high-yield industrial oil and gas flow obtained from the 8,200 m Cambrian subsalt dolomite reservoir in Well L1, the deepest well in Asia, further proves that this area has great potential. Du et al. (2016) consolidated seismic data interpretation, drilling, and geological data of the outcrop on the periphery of the basin to investigate the petroleum and geological conditions such as source, reservoir, and cap of the Cambrian subsalt dolomite in the Tarim Basin. Ni et al. (2017) investigated the characteristics and main controlling factors of the Cambrian subsalt dolomite reservoir in the middle-eastern Tarim Basin and considered that the main reservoir types of Cambrian subsalt dolomite in the middle Tarim Basin included intergranular pores and intergranular solution pores, dissolution pores, intergranular micropores, and natural fractures, and fractures were often combined with other kinds of pore types to form composite fracture-pore-type or fracture-vuggy-type reservoirs. Yin et al. (2015) established the calculation models of elastic modulus, Poisson's ratio, strength, and fracturing ability of the dolomite reservoir based on rock mechanics experiments and fine determination of rock components, analyzed the influences of rock mechanics parameters of different lithological components, established the *in situ* stress calculation model, determined detailed *in situ* stress section, calculated natural fracture cohesion, sliding friction coefficient, normal stress, and shear stress, and determined the opening rate under different injection pressure to optimize the fracturing construction interval, pumping procedure, segmented perforation cluster, construction pressure, etc. Previous research results have laid a rich theoretical foundation and reference for this study; however, they highlight the analysis of the geological characteristics and rarely focus on natural fractures and their mechanical characteristics and do not recognize that natural fractures are the main factor affecting the reservoir quality, resulting in defects in the understanding of reservoir quality.

Taking the Well L1 in the northern uplift as an example, this study uses imaging logging, core, rock, chip, and other data to identify and obtain the occurrence of natural fractures, define the characteristics of natural fractures, analyze the stress characteristics of natural fractures, calculate the natural fracture mechanical activity index, and establish a quality evaluation index for the dolomite reservoir with natural fractures, which consists of a geological mechanical activity index of natural fractures, width, length, and apparent porosity of natural fractures. The results can provide a reference for the optimization of reservoir acid–fracturing reformation parameters in this area and improve the understanding of reservoir quality and well completion reformation under similar geological conditions.

2 GEOLOGICAL SETTING

Located in the northern part of the Tarim Basin, the Northern Uplift is a long-term stable marine carbonate residual paleo uplift formed in the Middle Caledonian period on the background of basement paleo uplift. Multi-stage tectonic movement is the key to the formation of the Sinian–Cambrian tectonic pattern in this area. The tectonic background of a low uplift is developed in the Nanhua–Sinian system (Du et al., 2016; Yang et al., 2020). The period from Early Cambrian to Middle Ordovician was the development stage of the platform basin sedimentary transition zone. The period from Middle Caledonian to Middle Hercynian was the formation stage of the Lunnan low uplift. The period of Late Hercynian to the present day is the stable settlement period of the Lunnan low uplift (**Figure 1**). During the process of tectonic evolution, faults were continuously formed and associated with natural fractures, resulting in the reservoir generally containing natural fractures (Du et al., 2016; Cheng et al., 2020).

From bottom to top, the Cambrian system consists of the Lower Cambrian Yuertusi Formation (Є1y), Xiaoerbulake Formation (Є1x), Wusonggeer Formation (Є1w), Middle Cambrian Shayilike Formation (Є2s), Awatage Formation (Є2a), and Upper Cambrian Lower Qiulitage Formation (Є3xq). The Є1y Formation is a set of marine sediments dominated by black shale, thin-layer siliceous phosphatic nodule––bearing mudstone, and nodular limestone. The Є1x Formation comprises micritic limestone, spheroidal limestone, and a small amount of granular limestone. The Є1w Formation is interbedded with thin-middle argillaceous dolomite, argillaceous silty dolomite, and thin granular dolomite. The Middle Cambrian Є2s formation comprises medium thick dark gray and grayish brown argillaceous silty dolomite and granular dolomite, with a set of stably distributed limestone in the middle and upper part. The Є2a Formation develops in extremely thick evaporating lagoons or limited platform tidal flat faces which contain gypsum salt rock, gypsum mudstone, argillaceous dolomite, etc (Yang et al., 2020).

3 CHARACTERISTICS OF NATURAL FRACTURES

Taking Wells L1 and L3 as examples, this study explains the natural fracture development characteristics of the Cambrian subsalt dolomite reservoir in the Northern uplift. The Cambrian subsalt formations exposed by Well L1 are Є2s, Є1w, Є1x, Є1y, and Z3q of the Upper Sinian system. The Sinian system and Cambrian system of the Luntan 1 well have a small angle unconformity contact relationship. The L1 well was drilled and exposed a set of source rocks and two sets of reservoir-cap rocks below the Cambrian salt. The first reservoir–cap combination comprises the Є2s–Є1w formation which contains dolomite and overlying awatag formation gypsum. The gypsum layer is 230 m thick, and the thickness of single-layer gypsum is 10~15 m. The other reservoir–cap combination comprises the dolomite weathering crust karst reservoir of the Sinian Z3q formation and overlying Є1y formation mudstone (Yang et al., 2020), **Figure 2**.

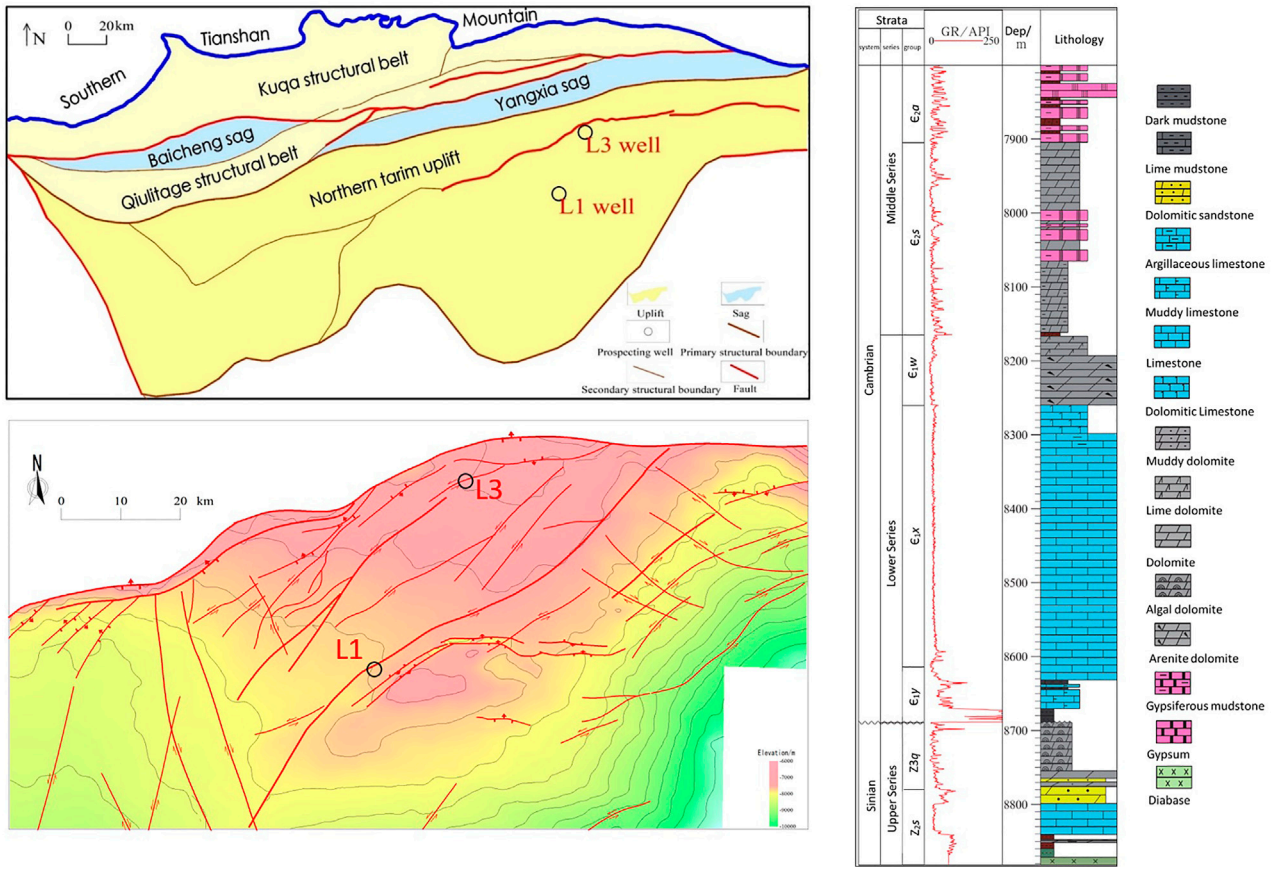

FIGURE 1 | Tectonic location and lithology.

The down well cores were taken out from 8,641–8,649.5 m of the well L1 in Є1y formation. The lithology is mainly dolomite, mudstone, calcareous mudstone, and lime-bearing mudstone with the horizontal bedding. Four horizontal micro-fractures fully filled with calcite, 16 horizontal micro-fractures fully filled with argillaceous rock, seven oblique micro-fractures fully filled with argillaceous material, and four vertical micro fractures fully filled with calcite are identified from the cures shown in **Figure 3**. Based on the systematic processing of the imaging logging data in Well L1, natural fractures were picked up manually, and 18 natural fractures were identified, which were distributed mainly in the Є2s formation of the Middle Cambrian and the Є1w formation of the Lower Cambrian (**Figure 3**).

In **Figure 3**, the left figure shows part core photos in 8,641–8,649.5 m of well L1, and the lithology and depth of the sampling are shown in **Figure 1**. Horizontal bedding (yellow arrow) and micro-natural fractures (green arrow) can be clearly identified in the figure. The linear density of natural fractures reaches 2.8/m, but these natural fractures are fully filled with calcite, and these natural fractures are not identified in the imaging logging of this section. The middle figure shows the image of some natural fractures in 7,904~8044 m. Seven natural fractures are picked up in this section. The strike of group 1 is near NS, and the other two groups are NE 22.33° ~ 54.79°. It can be seen in the FMI image that these natural fractures have not been filled. The right figure shows the image of some natural fractures in 8,195 ~ 8,260.5 m. Eleven natural fractures are picked up in this section. There are three natural fractures with a strike of NE 26.3° ~ 4.31 °and eight fractures of NE 50°. From the FMI image, it can be seen that these natural fractures have not been filled too.

Geological research shows that the natural fractures were formed in the middle to late Caledonian movement. At the same time, due to the strong fault activity in the Early Hercynian period, the natural fractures continued to develop and transformed to the current state (Du et al., 2016; Yang et al., 2020).

The stratum drilled in well L3 (35.2 km away from L1) is completely consistent with that in well L1. The hydrocarbon source rock in this region is Cambrian Є1y formation, with good oil and gas display. Through core observation, the stratum in this section is mainly black mudstone and gray dolomite, with micro pores and micro fractures locally, and the overall fractures are not developed. From electrical imaging data, five natural fractures are picked up, with the strike mainly from northeast to southwest, and the dip angle is 35–64°, which are medium and low angles. The angle between the fracture strike and principal stress orientation (NE 60°) is 20–50°, **Figure 4**.

From the principle of the likelihood of activation of natural fractures, it can be seen that the smaller the angle between the natural fracture trend and the current horizontal principal stress orientation (NE 54°), the easier it is to be activated and vice versa.

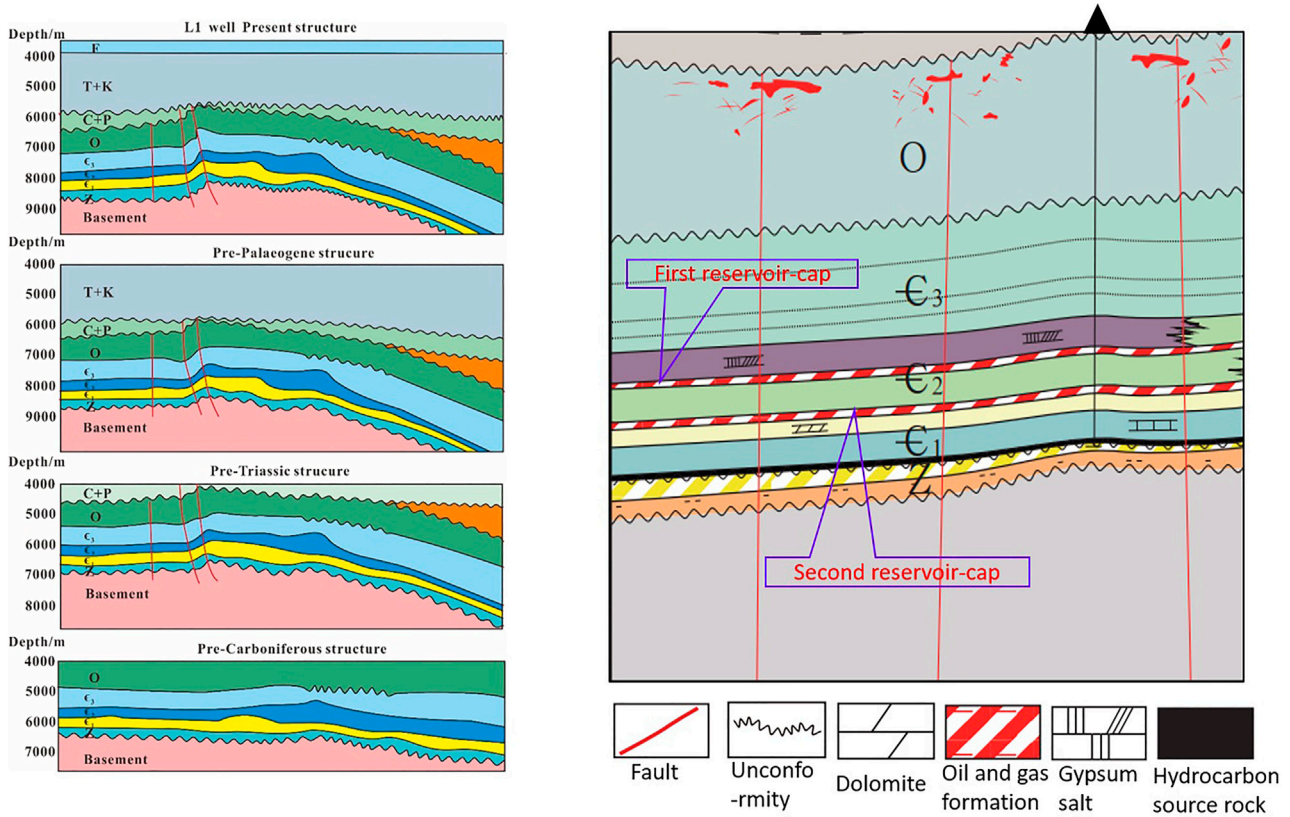

FIGURE 2 | Hydrocarbon accumulation mode of Well L1.

The contact relationship between hydraulic fractures and natural fractures depends on *in situ* stress, natural fracture cohesion, friction coefficient, etc., which is more complex without discussion in this article (Fisher et al., 2001; Potluri et al., 2005; Mohammed et al., 2011; Zeng et al., 2021).

Based on FMI image decomposition, bilateral resistivity, and other technical methods (Luthi and Souhaite, 1990; Xu, 2010), parameters such as fracture length (FraL), mean hydraulic aperture (FraW), and fracture apparent porosity (FraP) were calculated in this study (**Table 1**).

4 MECHANICAL CHARACTERISTICS OF NATURAL FRACTURES AND CLASSIFICATION

4.1 Calculation of Rock Mechanical Parameters

As for the mechanical parameter calculation of natural fractures, it is necessary to accurately obtain the rock Poisson's ratio ν, internal friction angle CFA, Young's modulus E, compressive strength UCS, shear strength USHE, shear modulus G, bulk modulus K, and other parameters. On the basis of the rock mechanics experiments, the dynamic–elastic parameters of rocks by analyzing the longitudinal and transverse wave velocity data measured at the same time in the experiment were obtained, and the calculation model of the rock force field parameters and the dynamic and static conversion models of the rock elastic parameters suitable for the Cambrian subsalt dolomite reservoir were established (Zoback, 2007).

The calculation model of compressive strength is as follows (**Eq. 3-1**):

$$UCS = 2\sqrt{1-\sin^2(CFA)} \times \frac{USHE}{1-\sin(CFA)}, \qquad (3-1)$$

where UCS is the uniaxial compressive strength; CFA is the internal friction angle; and USHE is the shear strength.

The internal friction angle can be calculated by **Eq. 3-2**.

$$CFA = (\pi/12) \cdot \left(2 \times \left(1 - \frac{\nu}{1-\nu}\right) + 1\right), \qquad (3-2)$$

where ν is Poisson's ratio.

The shear strength (USHE) may be calculated based on **Eq. 3-3**.

$$USHE = 0.025 \times E \cdot K \cdot (0.008 \cdot V_{sh} + BCC \cdot (1 - V_{sh})) \times 1.020245 \times 10^{-4}, \qquad (3-3)$$

where E is the elastic modulus; K is the bulk modulus; BCC is the inherent strength coefficient of the rock, and the value of

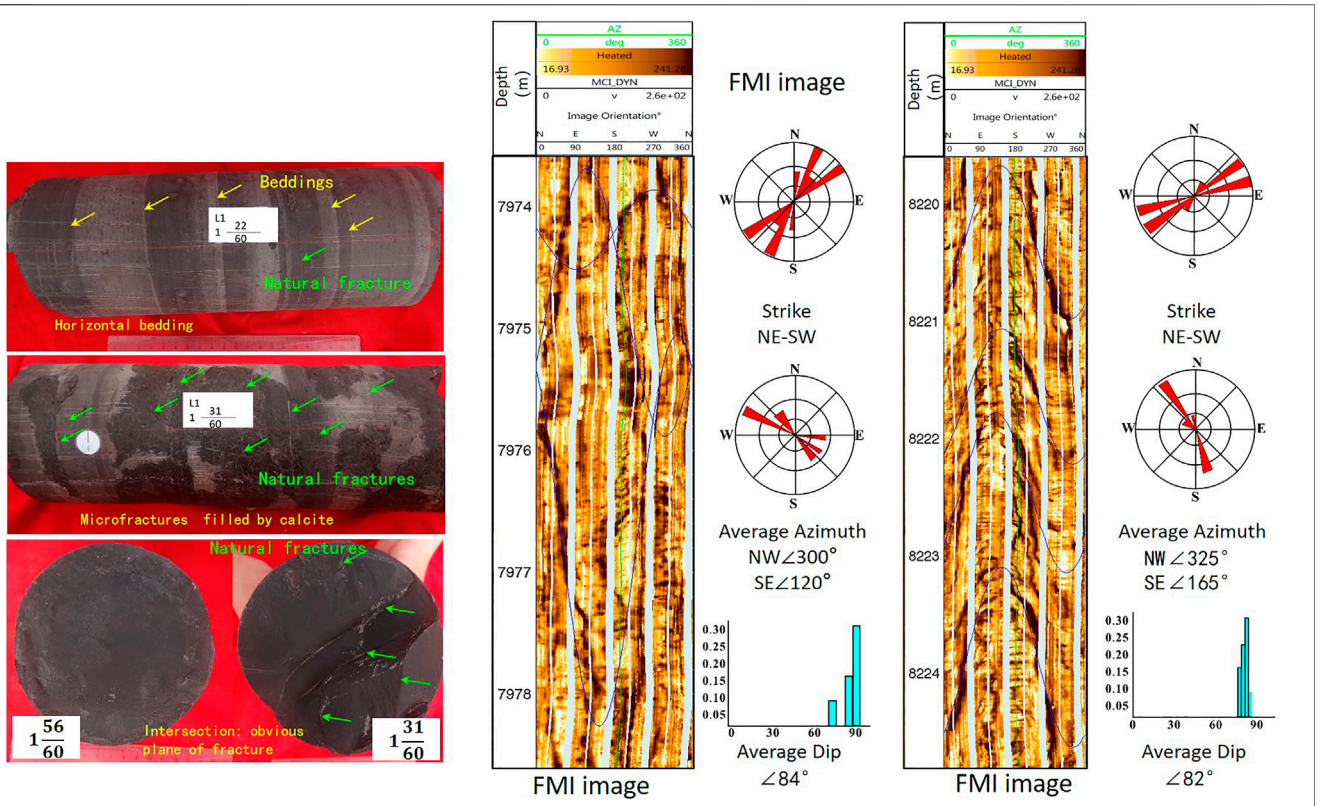

FIGURE 3 | Cores, imaging logging photos, and natural fracture orientations in Well L1. This figure contains three parts, the left are core pictures from 8,641–8,649.5 m of well L1, Є1y formation, and the source rock. The right parts are the FMI image and natural fractures picked up from FMI logging in 7,904~8044 m and 8,195~8,260.5 m, respectively.

the dolomite reservoir is 0.002; V_{sh} is the volume content of mudstone.

The calculation of Young's modulus and Poisson's ratio is based on the conventional calculation model (Zoback, 2007; Chen et al., 2008; Lu et al., 2015). Through the rock mechanics experiment (Yin et al., 2015), the dynamic and static conversion between Young's modulus and Poisson's ratio is regressed and fitted as follows (**Eq. 3-4**, **Eq. 3-5**):

$$E_{sta} = 0.8424E_{dyn} - 11.089, \quad (3-4)$$

$$\nu_{sta} = 0.9696\nu_{dyn} + 0.0149, \quad (3-5)$$

where E_{sta} is static Young's modulus, E_{dyn} is dynamic Young's modulus, ν_{sta} is static Poisson's ratio, and ν_{dyn} is dynamic Poisson's ratio.

4.2 Establishment of the 1D Geomechanics Model

4.2.1 Determination of Azimuth of Horizontal Maximum Principal Stress

The azimuth of the horizontal maximum principal stress is the important data to calculate the mechanical characteristics of the natural fractures. There are three methods to identify the orientation of the horizontal maximum principal stress: 1) dipole shear wave anisotropy (derive from dipolar shear wave logging). 2) Shear breakout direction statistics of the wellbore (derived from the resistivity imaging logging or dip angle well logging). 3) Drilling-induced fracture strike picked up from the wellbore (derived from resistivity imaging logging) (Cai, et al., 2015; Zoback, 2007).

4.2.2 Calculation of Stresses

The *in situ* stress field in the reservoir is characterized by a third-degree, second-order tensor, which includes three normal stresses and six shear stress components in any Cartesian coordinate system. The shear stress is symmetrical about the diagonal. When the coordinate axis is parallel to the three principal stress directions, the shear stress is zero, and the eigenvalue and eigenvector of the stress tensor correspond to the magnitude and direction of the principal stress, respectively (**Eq. 3-6**). At this time, the stress state at any point in the deep crust can be described using one vertical stress and two horizontal stresses mutually perpendicular to each other. This view holds true in the range from the Earth's surface to the depth of 20 km of the crust (Zoback, 2007). Therefore, for the oil and gas reservoirs found in the Kelasu tectonic belt, the stress state at its corresponding position can be fully described with three principal stresses (vertical stress, σ_V; horizontal maximum principal stress, σ_H; and horizontal minimum principal stress, σ_h) and the azimuth of the horizontal principal stress.

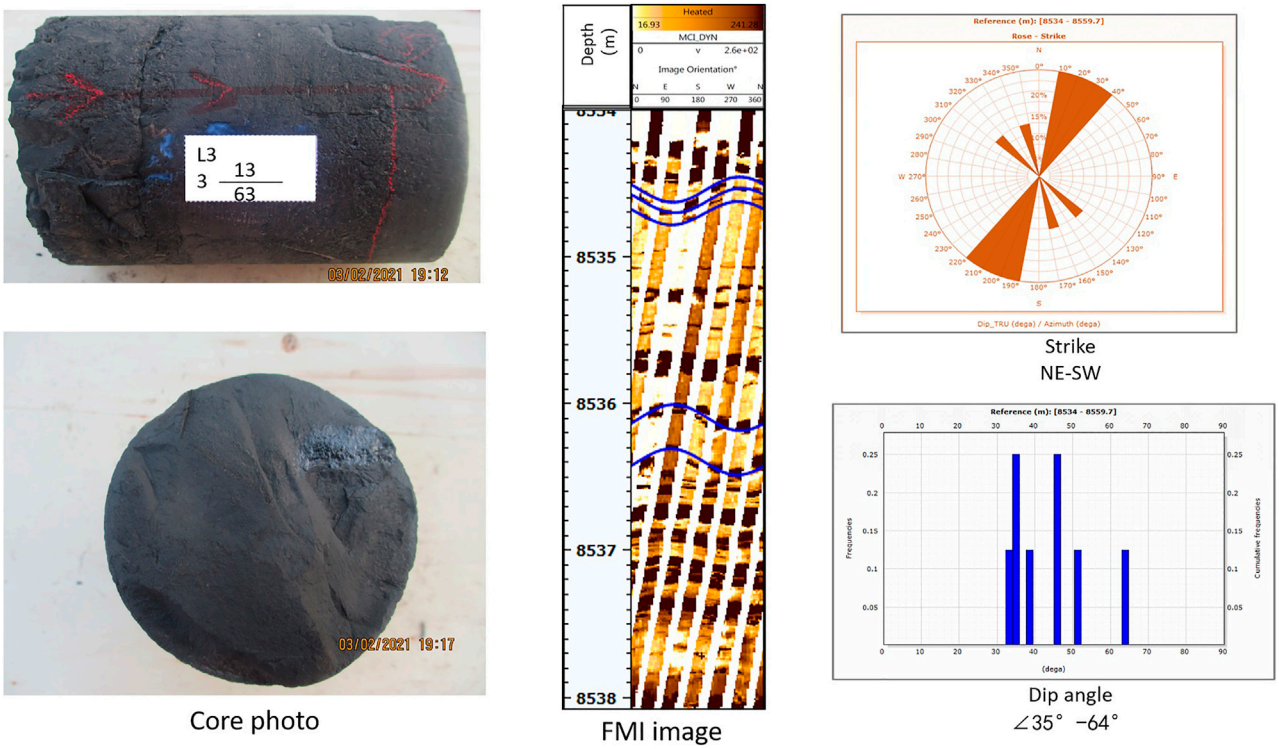

FIGURE 4 | Cores, imaging logging photos, and natural fracture orientations in Well L3. The left picture shows part core photos. An open horizontal natural fracture can be seen, which is consistent with the natural fracture picked up by FMI logging in this section (the right picture). These natural fractures have poor transverse continuity and short longitudinal extension distance, with a medium-to-low dip angle. The effectiveness of natural fractures is poor according to these characteristics (Gong et al., 2019; Gong et al., 2021).

TABLE 1 | Calculated natural fracture parameters of well L1.

No.	Depth (m)	Azimuth (°)	Strike (°)	Dip angle (°)	FraL (m)	FraW (mm)	FraP (%)
1	7,963.96	122.47	32.47	84.37	1.870	2.792	10.928
2	7,966.96	292.33	22.33	84.61	0.960	1.401	5.600
3	7,969.36	323.09	53.09	82.96	0.940	1.376	2.638
4	7,971.86	314.15	44.15	83.15	0.310	0.453	1.560
5	7,974.19	92.64	2.64	70.38	0.929	1.348	2.732
6	7,974.79	296.17	26.17	83.73	0.945	1.371	1.806
7	7,976.66	144.79	54.79	86.37	0.072	0.105	3.169
8	8,217.15	320.56	50.56	81.14	0.945	1.430	1.910
9	8,218.59	309.03	39.03	82.05	0.934	1.413	0.548
10	8,220.32	321.84	51.84	78.92	0.929	1.405	1.459
11	8,221.64	325.77	55.77	77.55	0.967	1.464	1.651
12	8,222.46	310.31	40.31	79.26	0.970	1.468	0.209
13	8,223.86	326.97	56.97	80.32	0.496	0.750	0.501
14	8,234.56	296.3	26.3	81.79	0.963	1.421	0.116
15	8,247.75	347.55	77.55	80.87	0.943	1.390	0.251
16	8,253.66	167.69	77.69	82.65	0.943	1.390	0.137
17	8,258.25	162.06	72.06	84.63	0.963	1.421	0.001
18	8,258.85	164.61	74.61	84.43	0.948	1.398	0.150

$$\sigma = \begin{bmatrix} \sigma_{11} & \sigma_{12} & \sigma_{13} \\ \sigma_{21} & \sigma_{22} & \sigma_{23} \\ \sigma_{31} & \sigma_{32} & \sigma_{33} \end{bmatrix} = \begin{bmatrix} \sigma_H & 0 & 0 \\ 0 & \sigma_h & 0 \\ 0 & 0 & \sigma_v \end{bmatrix}. \quad (3-6)$$

The most important significance of the three principal stresses in **Eq. 3-6** is that their relationship determines the stress state of the reservoir. When faults within the crust are in a stable state, the

ratio of the maximum to minimum principal stress will meet **Eq. 3-7** (Jaeger and Cook, 1979).

$$\frac{\sigma_{\max}}{\sigma_{\min}} = \left[\left(\mu^2+1\right)^{1/2}+\mu\right]^2. \quad (3-7)$$

According to Anderson's fault and the stress classification model, when the vertical stress is at the maximum, intermediate, and minimum stress, respectively, *in situ* stress within the reservoir is the stress state of potential normal fault type, strike–slip type, and reverse fault type, correspondingly. The specific *in situ* stress state controls the mechanical behavior of geological bodies such as fractures and faults in the reservoir and affects the reservoir permeability and fluid-flow characteristics, which is the most direct correlation between the magnitude and direction of *in situ* stress and oil and gas exploration and development.

Zoback (2007), Liu and Luo (2005), and Chen (2008) had proposed the mathematical model for calculating triaxial stresses using logging data. The vertical stress value is equivalent to the gravity of overlying strata. Therefore, through the rock density integration from the surface to the target depth z, the mean density of the interval above the starting depth of density logging z_0 is determined according to the adjacent wells and regional formation lithology, and then σ_V is calculated according to **Eq. 3-8**.

$$\sigma_V = \int_0^z \rho(z)gdz \approx \bar{\rho}gz_0 + \int_{z_0}^z \rho(z)gdz. \quad (3-8)$$

Hydraulic acid-fracturing construction data are used to determine the σ_h at a specific location. Taking these measured data as the constraint basis, in combination with the elastic stress model (Prats, 1981) considering multiple factors such as overlying load, thermal strain, and tectonic strain (**Eq. 3-9**), the one-dimensional (1D) continuous reservoir σh section is calculated.

$$\sigma_h = \frac{\nu}{1-\nu}\sigma_v - \frac{\nu}{1-\nu}\alpha P_p + \alpha P_p + \frac{E}{1-\nu^2}\varepsilon_h + \frac{\nu E}{1-\nu^2}\varepsilon_H, \quad (3-9)$$

where ν is Poisson's ratio, α is Biot pore elasticity coefficient, Pp is pore pressure, and ε_H and ε_h are the strain in the direction of maximum and minimum horizontal principal stress, respectively.

For the horizontal maximum principal stress, Barton and Zoback (1988) believed that under the specific horizontal stress state, rock strength, and wellbore pressure, a fracture trace with a certain collapse width will be formed, that is, during the drilling process, the shear collapse may continuously deepen to the radial direction for a certain time, but the collapse width will remain stable. Hence, the calculation method is as shown in **Eq. 3-10**:

$$\sigma_H = \frac{\left(C_0 + 2P_p + \Delta P\right) - \sigma_h\left(1+2\cos\phi\right)}{1-2\cos\phi}, \quad (3-10)$$

where C_0 is the compressive strength of the rock in the stratum and φ is the collapse width of the borehole wall. The method is to obtain the reliable σ_h and σ_H at the specific position of the wellbore. Then, the data at these key points are used to realize the continuous calculation of the horizontal maximum and minimum principal stresses in the 1D section based on **Eq. 3-11**, which will provide the basis for the calculation of the stress characteristic parameters of natural fractures.

$$\sigma_H = \frac{\nu}{1-\nu}\sigma_v - \frac{\nu}{1-\nu}\alpha P_p + \alpha P_p + \frac{\nu E}{1-\nu^2}\varepsilon_h + \frac{E}{1-\nu^2}\varepsilon_H. \quad (3-11)$$

When analyzing the stress characteristics of natural fractures, it is also necessary to consider the angle between the horizontal maximum principal stress and natural fractures. In this article, three methods, that is, fast shear wave azimuth, drilling induced fracture, and borehole wall stress collapse imaging are used to obtain the *in situ* horizontal maximum principal stress direction (Yin et al., 2015).

4.3 Mechanical Activity Evaluation of Natural Fractures and Quality Classification of Fractured Reservoirs

For the evaluation of the mechanical activity of faults and fractures, Amontons (Otsuki and Matsukawa, 2013) proposed that friction sliding would occur when the ratio of shear stress to normal stress on the structural plane exceeded its friction coefficient based on Da Vinci's friction experiment. Coulomb (1973) proposed the Coulomb failure function, which succinctly expressed the activity characteristics of the primary fracture surface caused by friction and sliding (Zoback et al., 2012, 2007; Jiang et al., 2021; Gong et al., 2021). The Coulomb failure function (CFF) is shown in **Eq. 3-12**:

$$CFF = \tau - \mu\sigma_n. \quad (3-12)$$

When the CFF is negative, the fracture surface remains stable, and the shear stress is not enough to overcome the sliding resistance. However, when the CFF reaches or exceeds zero, the shear stress overcomes the normal stress on the primary fracture surface, resulting in friction sliding.

From **Eq. 3-12**, we may see that the ratio of shear stress to normal stress in a fracture plane τ/σ_n is an important indicator of the mechanical activity of natural fractures. Barton and Zoback (1994), Barton and Zoback (1995) confirmed that faults and fractures with better potential activity have better permeability. Townsend and Zoback (2000) proposed that the hydraulic conductivity of faults did not depend on the effective normal stress acting on the fault plane but on the ratio of shear stress to effective normal stress. When studying the Suban gas field in South Sumatra, Indonesia, Hennings et al. (2012) also mentioned that the ratio of shear stress to normal stress τ/σ_n is one of the factors affecting the permeability of fractured reservoirs. Through the aforementioned methods, they obtained the occurrence data of natural fractures and the *in situ* stress value of natural fractures and then analyzed the normal stress and shear stress of natural fracture surfaces as well as their ratios.

The Coulomb friction criterion is used to judge the sliding of a fault unit. Assuming that the change of fluid pressure causes the change of fault activity, we can calculate the critical pore pressure, and any value exceeding this pore pressure may cause activity along the fault surface (Zoback et al., 2012,2007; Jiang et al., 2021). When the change in the pore pressure causes the sliding of the fault, in which, the CFF is zero, **Eq. 3-12** will be changed to

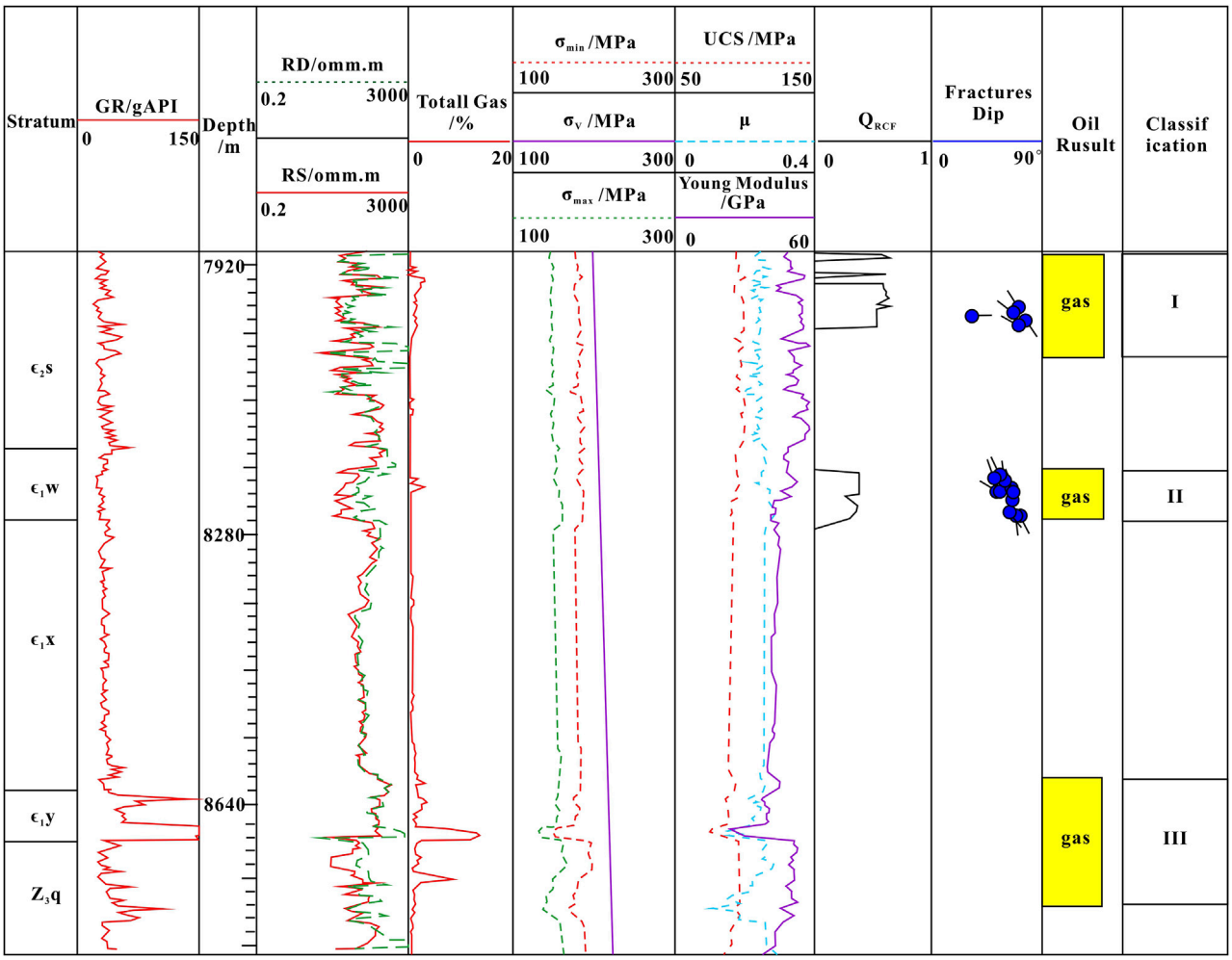

FIGURE 5 | Geomechanical interpretation and reservoir classification in Well L1. It can be seen that the logging interpretation of the reservoir of the third section (yellow filled rectangle) is a gas reservoir, but there are great differences in the geomechanical parameters. The first section is defined as Class I with lower *in situ* stress, five natural fractures, and higher Q_{RCF} , the second section is Class II with higher stress, medium Q_{RCF}, and 11 natural fractures. The GR ray of the third section changes violently, and the lithology is mainly mudstone and argillaceous limestone, and the stress is high in general, but there is a lower stress section in the middle, but no natural fracture is picked up, which is defined as Class III.

$$\tau - \mu\left(\sigma_n - P_p\right) = 0. \tag{3-13}$$

If the aforementioned pore pressure is defined as the critical pore pressure of fault activity, **Eq. 3-14** will be obtained:

$$P_p^{crit} = \sigma_n - \frac{\tau}{\mu}. \tag{3-14}$$

This study normalizes the two attributes with the range transformation method and then puts forward a new fracture geomechanical activity calculation model, namely, the Fractures Geomechanical Activity Index (FGAI) (Cai et al., 2015; Jiang et al., 2021), which is suitable for areas with high stress, high pore pressure, and complex structure:

$$FGAI = \sum_{i=1}^{2} W_i G_i, \tag{3-15}$$

where Gi is the normalized value of different geological attributes and G_1 is the ratio of shear stress to normal stress of the fracture surface τ/σ_n. G_2 is the critical pore pressure of fault sliding. Wi is the weight coefficient of each geological attribute. Therefore, the FGAI is expressed as **Eq. 3-16**:

$$FGAI = W_1 \frac{\tau/\sigma_n - \tau/\sigma_{n\min}}{\tau/\sigma_{n\max} - \tau/\sigma_{n\min}} + W_2 \frac{P_{p\max}^{Crit} - P_p^{Crit}}{P_{p\max}^{Crit} - P_{p\min}^{Crit}}, \tag{3-16}$$

where the parameters with subscripts “max” and “min” are the maximum and minimum values of the aforementioned two geological parameters in the region, respectively, and the weight of the two parameters meets W1 + W2 = 1. The value range of the FGAI is 0~1. When the value is greater, the potential activity of the fault is stronger. The calculation process of this index comprehensively considers the regional *in situ* stress field, reservoir pore pressure, rock mechanical properties, and fracture

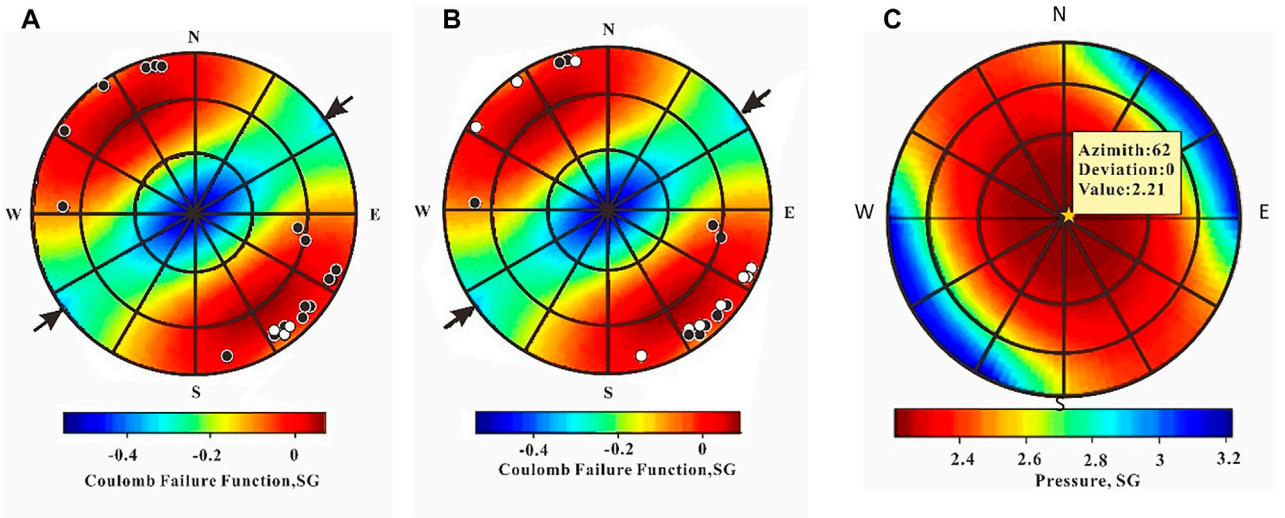

FIGURE 6 | Modeling results showing the critical fracture opening pressure in Well L1. This figure is called stereographic (Zoback 2007). The opening pressure of reservoir **Section 2** and reservoir **Section 3** is simulated together. When the injection pressure is simulated to 1.61 sg, the natural fractures of the first section are activated **(A)**. When the injection pressure is simulated to 1.82 sg, the natural fractures of the second section are activated **(B)**, indicating that the natural fractures of the first section of the reservoir are easier to be stimulated, and the potential mechanical activity is better. There are no natural fractures in the third section in which the critical opening pressure of the matrix reservoir is simulated **(C)**. The results are shown in **Table 1**.

TABLE 2 | Acid-fracturing reformation design in Well L1.

Section No.	Depth (m)	Q_{RCF}	Class	Equivalent circulating density (SG)	Pumping rate (m^3/min)	Total fluid volume (m^3)	Total porosity (%)	Gas saturation (%)
1	7,904.5~8,044	0.63	I	1.61	5	600	3~5	65~68
2	8,195.3~8,260.5	0.42	II	1.82	5	1,000	3.1~3.5	66~72
3	8,606.7~8,777.8	0	III	2.21	5	800	3.8~4.1	75

geometric occurrence, directly reflecting the potential mechanical activity and behavior of natural fractures under the control of the *in situ* stress field.

4.4 Quality Classification of Reservoir Containing Natural Fractures

The authors have exploited the method to estimate the quality about the reservoir containing natural fractures. From the aforementioned method, length of natural fracture (FraL), width of fracture (FraW), apparent porosity of fracture (FraP), and mechanical activity index (FGAI) were obtained using logging data. From the significance of the characterization of these parameters, they all indicate a positive impact on reservoir quality. Therefore, the fractured reservoir quality index is defined as **Eq. 3-17**:

$$Q_{RCF} = W_1\frac{FGAI - FGAI_{\min}}{FGAI_{\max} - FGAI_{\min}} + W_2\frac{FraL - FraL_{\min}}{FraL_{\max} - FraL_{\min}} + W_3\frac{FraW - FraW_{\min}}{FraW_{\max} - FraW_{\min}} + W_4\frac{FraP - FraP_{\min}}{FraP_{\max} - FraP_{\min}}, \quad (3-17)$$

where the parameters with subscripts "max" and "min" in the formula are the maximum and minimum values of the aforementioned four geological parameters in the region, respectively. The parameter weight meets W1+ W2+W3+W4 = 1, and the value range of the reservoir quality index is 0~1.

In this study, the reservoir quality index Q_{RCF} is used to divide the reservoir into three categories: Class I reservoir is 0.6 ~ 1, Class II reservoir is 0.3~0.6, and Class III reservoir is less than 0.3. For a fractured reservoir, if there are no natural fractures in a certain stratum, the Q_{RCF} is zero, and then the reservoir quality will be determined to be Class III.

5 APPLICATIONS IN HYDRAULIC PROGRAM OPTIMIZATION

5.1 Design of an Acid-Fracturing Stimulation Scheme

The aforementioned method is used to analyze the Cambrian subsalt dolomite of Well L1, obtain rock strength, Young's modulus, triaxial stress, and reservoir quality index Q_{RCF}, and

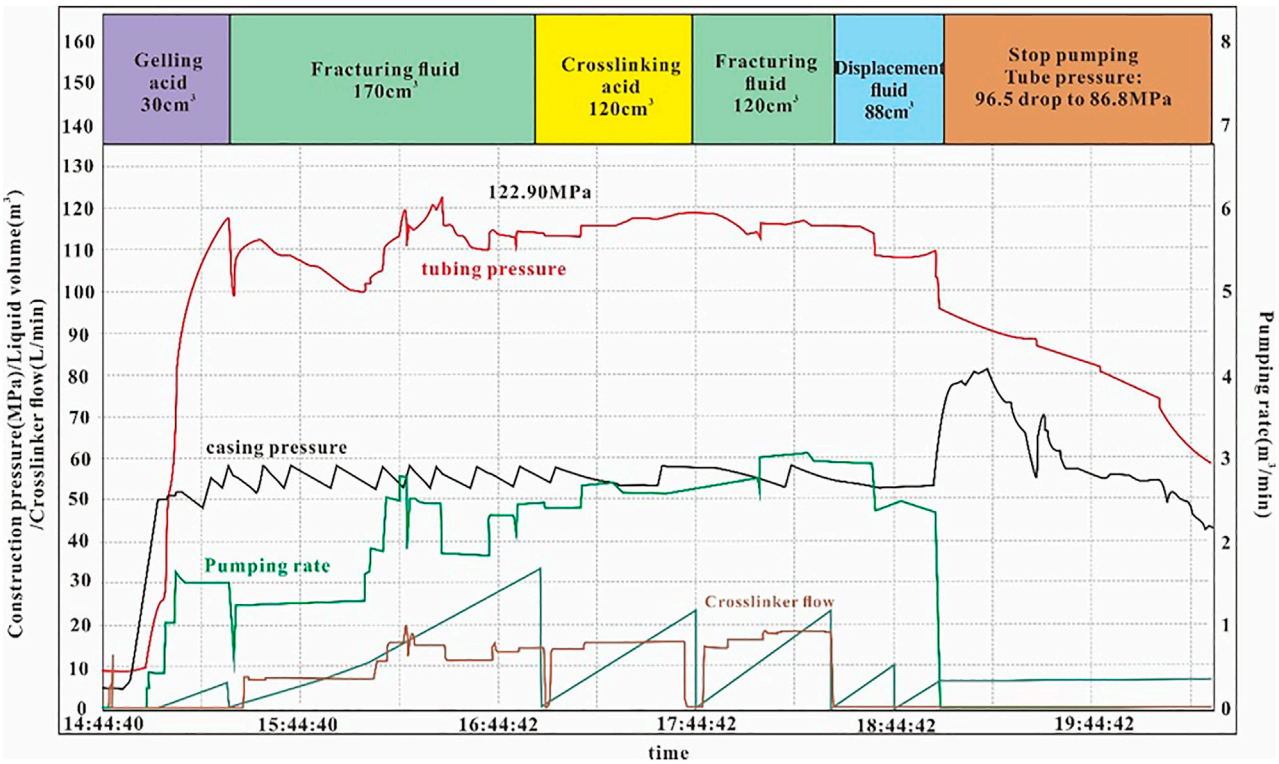

FIGURE 7 | Curve of the acid-fracturing stimulation in 8,606.7–8,777.8 m (**Section 4**), and the relationship between tubing pressure and pumping rate shows that acid-fracturing fluid is constantly squeezed into the formation due to high porosity, but there is no hydraulic fracture newly generated.

the reservoir quality according to the Q_{RCF} calculation model and the natural fracture petrophysical data in **Table 1**. In **Figure 5**, from left to right, the formation name, GR, depth, resistivity, gas logging display, triaxial stresses, compressive strength, Poisson's ratio, Young's modulus, natural fractures, oil and gas interpretation, conclusion, and reservoir quality are represented in each track, respectively. Based on logging interpretation, the reservoirs in 7,904.5–8044, 8,195.3–8,260.5, and 8,606.7–8,777.8 m are gas reservoirs. Among the three sections, the mean values of the first and second sections are 0.63 and 0.42, respectively. Since no fracture is picked up in the third reservoir, the Q_{RCF} value is 0. Therefore, the reservoir quality of the three reservoirs is divided into Class Ⅰ, Class Ⅱ, and Class Ⅲ, respectively.

Based on oil and gas expressions and logging interpretations, three sections are optimized for acid-fracturing reformation. For designing the acid-fracturing reformation scheme, it is necessary to predict the hole–bottom pressure additionally. The critical opening pressure of each natural fracture is calculated using the method described previously. In **Figure 6**, green dots represent opening natural fractures in the original state, white dots represent some under the current injection pressure, and black dots represent the others which are not stimulated (Zoback, 2007). **Figure 6A** shows the equivalent mud density of the natural fracture opening pressure in 7,904.5–8044 m, which is 1.61 SG, and **Figure 6B** shows the equivalent mud density of the natural fracture opening pressure about 8,195.3–8,260.5 m, which is 1.82 SG. Since there is no natural fracture in the third reservoir 8,606.7–8,777.8 m, the matrix hydraulic fracturing pressure is comprehensively affected by pore pressure, *in situ* stress, and rock mechanical parameters. The fracture initiation pressure equivalent mud density is simulated to 2.21 SG, shown in **Figure 6C** (Zoback 2007), indicating that the formation in this section is difficult to be fractured. Then, according to the rock mechanics and *insitu* stress parameters obtained from the wellbore, this study simulated the parameters such as pumping procedure, pumping rate, and acid solution consumption under the optimal capacity conditions and finally designed the acid-fracturing reformation scheme for three sections in Well L1 (**Table 2**). Generally, the stress shadow needs to be considered in the parameter design of acid-fracturing operation (Chun et al., 2009; Cai et al., 2017; Yu et al., 2017). Due to large reservoir space in the three sections and general construction, the influence of the stress shadow is small and will not be considered.

5.2 Analysis of Acid-Fracturing Results

The total fluid amount squeezed into the third section is 528 m^3, with the pumping rate of 0.41~3 m^3/min and the pump pressure of 12.5~122.9/115.4 MPa. When the pumping is stopped to measure the pressure drop, the tubing pressure decreased from 96.5 to 86.9MPa, **Figure 7**. For the second reservoir with hydrochloric acid, the parameters are as follows: acid concentration: 20%, viscosity: 30mPa/s, density: 1.10 SG, acid consumption: 450 m^3, consumption of fracturing fluid: 460 m^3,

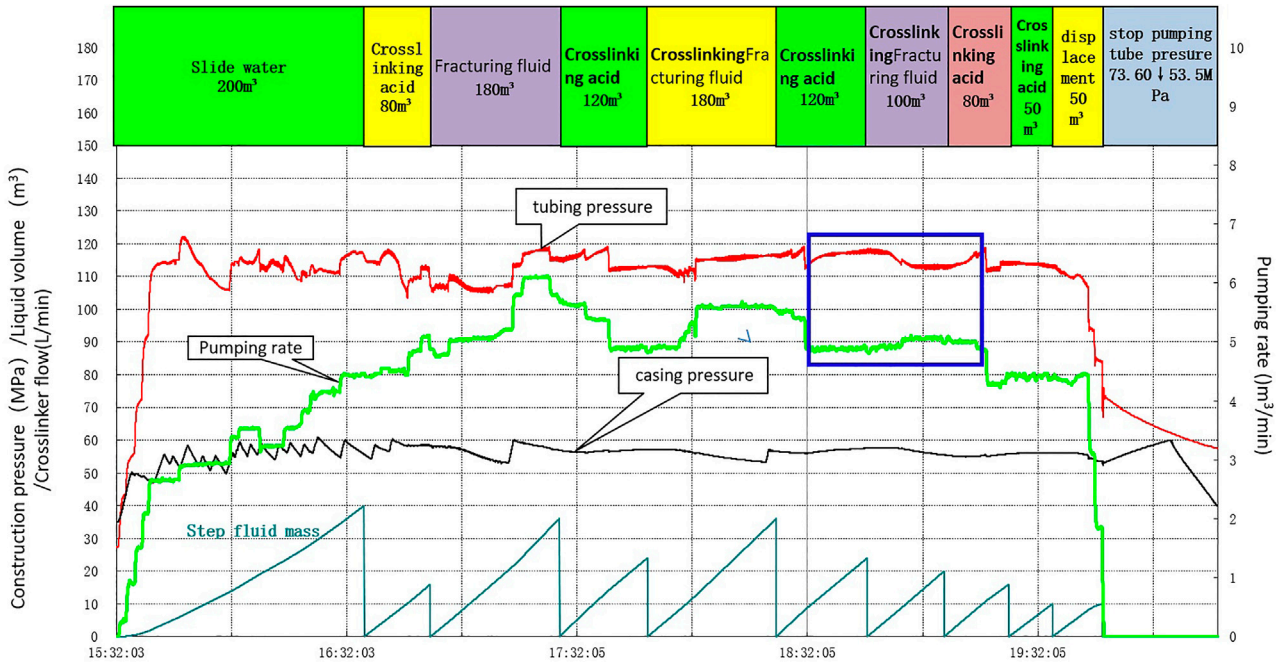

FIGURE 8 | Curve of the acid-fracturing stimulation in 8,203.00–8,260.00 m (**Section 3**), and the relationship between tubing pressure and pumping rate described in the blue rectangular box indicates that when the pumping rate is stable, the tubing pressure increases and then decreases, and when the pumping rate increases, the tubing pressure is lower, indicating that the formation is stimulated to generate new hydraulic fractures or the pre-existing natural fractures are activated.

pump pressure: 33.6–122.1/111.5 MPa, casing pressure: 36.1–60.7/55.6 MPa, pumping rate of 0.3–6.12/4.54 m^3/min, and total fluid amount squeezed into the formation is 1,116.4 m^3. The first reservoir adopts the same acid system, with acid consumption of 350 m^3, fracturing fluid consumption of 120 m^3, pump pressure of 32.1–125/113.1 MPa, casing pressure of 37.2–60.2/55.84 MPa, pumping rate of 0.53–8.16/5.87 m^3/min, and the total fluid amount is 660 m^3.

It can be determined from the acid-fracturing construction curve (**Figure 7**) that the third reservoir is far from reaching the designed construction scale, the formation has not been fractured, and the output has not been obtained in the later production. As mentioned previously, the total porosity and gas saturation of this formation are the highest among the three. However, due to the lack of natural fractures and low reservoir quality, high production is not obtained after acid-fracturing, expectantly. The second and first sections are basically constructed according to the design parameters. After the pump is stopped, the tubing pressure decreases from 73.6 to 53.5 MPa (**Figure 8**), which means a sharp pressure drop and fractured formation. In the later stage, the oil output is calculated by changing the nozzle. Oil extraction in the second and first sections is carried out together, and under a 6-mm nozzle, tubing pressure is kept at 13MPa and the average daily oil output is 90 m^3 so as to obtain high-yield industrial oil and gas production.

Based on the analysis of the application results of Well L1, the combination of Q_{RCF} values obtained by integrating the mechanical parameters and petrophysical parameters of natural fractures can distinguish the differences in the quality of the Cambrian subsalt dolomite reservoir. For the reservoirs that are determined into Class III, the formation cannot be fractured under the current industrial conditions of acid-fracturing reformation; they can be abandoned in the selection of fracturing reformation sections. Due to the lack of microseismic monitoring during fracturing and repeated imaging logging data after fracturing, the fracture net patterns after acid-fracturing cannot be evaluated, which is the direction of study in the future.

6 CONCLUSION

1) Natural fractures can continuously develop in the Cambrian subsalt dolomite reservoir with a burial depth of more than 8,000 m in the northern uplift of the Tarim Basin. They are not unevenly distributed, showing the characteristics of segmental development. The strike of natural fractures intersects with the horizontal principal stress azimuth at a small angle.
2) The 1D geomechanics is established based on logging data to analyze mechanical characteristics of natural fractures and define and calculate the mechanical activity index FGAI of natural fractures, which is further used as a key indicator to determine the likelihood of the potential mechanical activity of natural fractures.
3) In combination with the length, hydraulic aperture, apparent porosity, and FGAI of natural fractures, a reservoir quality characterization parameter Q_{RCF} for ultra-deep fractured reservoirs is established, consisting of four normalized parameters.

4) The practical application shows that the Q_{RCF} can relatively and accurately distinguish the quality difference of the ultra-deep Cambrian subsalt dolomite reservoir. Sufficient consideration of reservoir quality classification during fracturing formation selection and construction parameter design will stimulate the high-quality reservoirs accurately and obtain a better performance.

DATA AVAILABILITY STATEMENT

The original contributions presented in the study are included in the article/Supplementary Material; further inquiries can be directed to the corresponding author.

AUTHOR CONTRIBUTIONS

GY, Conceptualization, Investigation, Writing—Original Draft; HZ, Supervision, Methodology, and Validation; YX, Software and Visualization; WZ, Formal Analysis; XW, Data Curation, Software; JL, Data Curation; SL, Formal Analysis.

FUNDING

This study is funded by the Major National Science and Technology Project (2016ZX05051), Major Science and Technology Project of PetroChina Company Limited (2018E-1803).

REFERENCES

Ameen, M. S., MacPherson, K., Al-Marhoon, M-I., and Rahim, Z (2012). Diverse Fracture Properties and Their Impact on Performance in Conventional and Tight-Gas Reservoirs, Saudi Arabia: The Unayzah, South Haradh Case Study. *AAPG Bull.* 96 (3), 459–492. doi:10.1306/06011110148

Barton, C. A., Zoback, M. D., and Moos, D. (1995). Fluid Flow along Potentially Active Faults in Crystalline Rock. *Geol* 23, 683–686. doi:10.1130/0091-7613(1995)023<0683:ffapaf>2.3.co;2

Barton, C. A., and Zoback, M. D. (1994). Stress Perturbations Associated with Active Faults Penetrated by Boreholes: Possible Evidence for Near-Complete Stress Drop and a New Technique for Stress Magnitude Measurement. *J. Geophys. Res.* 99, 9373–9390. doi:10.1029/93jb03359

Cai, B., Tang, B., and Ding, Y. (2014). Influence of Stress Shadow on Horizontal Well Fracturing[J]. *Nat. Gas. Ind.* 34 (7), 55–59. doi:10.3787/1000-0976.2014.07.009

Chen, M., Jin, Y., and Zhang, G. (2008). *Petroleum Engineering Rock Mechanics*. Beijing: Science Press.

Cheng, L., Zhong, L., and Liu, J. (2020). Diagenesis and Physical Properties of Subsalt Dolomite Reservoirs of the Cambrian, Bachu-Tazhong Areas, Tarim Basin [J]. *Oil Gas Geol.* 41 (2), 316–327. doi:10.11743/20200208

Coulomb, C. A. (1973). Surune application desregles demaximums etminimums a quelques problemes de statistique relatifs a larchitesture. *Acad. Roy." Sci. Mem. Mech. Min. Sci.* 7, 343–382.

Du, J., and Pan, W. (2016). Accumulation Conditions and Play Targets of Oil and Gas in the Cambrian Subsalt Dolomite, Tarim Basin, NW China [J]. *PETROLEUM Explor. Dev.* 43 (3), 327–339. doi:10.11698/PED.2016.03.0210. 1016/s1876-3804(16)30043-x

Fisher, Q. J., and Knipe, R. J. (2001). The Permeability of Faults within Siliciclastic Petroleum Reservoirs of the North Sea and Norwegian Continental Shelf. *Mar. Petroleum Geol.* 18, 1063–1081. doi:10.1016/s0264-8172(01)00042-3

Gong, L., Fu, X., Wang, Z., Gao, S., Jabbari, H., Yue, W., et al. (2019). A New Approach for Characterization and Prediction of Natural Fracture Occurrence in Tight Oil Sandstones with Intense Anisotropy. *Bulletin* 103 (6), 1383–1400. doi:10.1306/12131818054

Hennings, P., Allwardt, P., Paul, P., Zahm, C., Reid, R., Alley, H., et al. (2012). Relationship between Fractures, Fault Zones, Stress, and Reservoir Productivity in the Suban Gas Field, Sumatra, Indonesia. *Bulletin* 96 (4), 753–772. doi:10.1306/08161109084

Jaeger, J. C., and Cook, N. G. W. (1979). *Fundamentals of Rock Mechanics*. first edition. London: Chapman & Hall.

Jiang, T. W., Zhang, H., Xu, K., Yin, G. Q., Wang, H. Y., Wang, Z. M., et al. (2021). Technology and Practice for Quantitative Optimization of Borehole Trajectory in Ultra-deep Fractured Reservoir:a Case Study of Bozi A Gas Reservoir in Kelasu Structural Belt, Tarim Basin. *China Pet. Explor.* 26 (4), 149–161. doi:10.3969/j.issn.1672-7703.2021.04.001

Gong, L., Wang, J., Gao, S., Fu, X., Liu, B., Miao, F., et al. (2021). Characterization, Controlling Factors and Evolution of Fracture Effectiveness in Shale Oil Reservoirs. *J. Petroleum Sci. Eng.* 203, Article ID, 108655 pages. doi:10.1016/j.petrol.2021.108655

Liu, X., and Luo, P. *Rock Mechanics and Petroleum Engineering*. Beijing: Petroleum Industry Press,2004.

Lu, S. K., Wang, D., Li, Y. K., Meng, X. J., Hu, X. Y., and Chen, S. W. (2015). Research on Three-Dimensional Mechanical Parameters' Distribution of the Tight Sandstone Reservoirs in Daniudi Gasfield[J]. *Nat. Gas. Geosci.* 26 (10), 1844–1850.

Luthi, S. M., and Souhaite, P. (1990). Fracture Apertures from Electrical Borehole Scans. *Geophysics* 55 (3), 821–833. doi:10.1190/1.1890143

Ni, X., Huang, L., and Chen, Y. (2017). Characteristics and Main Controlling Factors of the Cambrian Pre-salt Dolomite Reservoirs in Tazhong Block, Tarim Basin[J]. *Oil Gas Geol.* 2017 (3), 489–498.

Otsuki, M., and Matsukawa, H. (2013). Systematic Breakdown of Amontons' Law of Friction for an Elastic Object Locally Obeying Amontons' Law. *Sci. Rep.* 3, 1586. doi:10.1038/srep01586

Potluri, N., Zhu, D., and Hill, A. D. (2005). Effect of Natural Fractures on Hydraulic Fracture Propagation, The SPE European Formation Damage Conference held in Scheveningen, The Netherlands, 25-27 May 2005. SPE 94568.

Prats, M. (1981). Effect of Burial History on the Subsuriace Horizontal Stresses of Formation Having Different Material Properties, *Society of Petroleum Engineers Journal*, 21, SPEJ658–662. doi:10.102118/9017-PA

Townend, J., and Zoback, M. D. (2000). How Faulting Keeps the Crust Strong. *Geology* 28 (5), 399–402. doi:10.1130/0091-7613(2000)028<0399:hfktcs>2.3.co;2

Xu, B., Li, Y., and Xiang, G. E. (2010). Analysis of Distributing Law and Influencing Factors of Compact Clastic Rock Fracture in Xujiahe Formation in West Sichuan Region [J]. *Well logging Tech. nology* 34 (5), 437–441.

Yang, H., Chen, Y., and Tian, J. (2020). Great Discovery and its Significance of Ultra-deep Oil and Gas Exploration in Well Luntan-1 of the Tarim Basin [J]. *China Pet. Explor.* 25 (2), 62–72. doi:10.3969/1672-7703.2020.02.007

Yin, G., Zhang, H., and Yuan, F. (2015). Geomechanical Characteristics of Dolomite Reservoir and its Application in Stimulation Optimization: an Example of East of Tazhong[J]. *Nat. Gas. Geosci.* 26 (7), 1277–1288. doi:10.11764/1672-1926.2015.07.1277

Yu, Y., Zhu, W., Li, L., Wei, C., Dai, F., Liu, S., et al. (2017). Analysis on Stress Shadow of Mutual Interference of Fractures in Hydraulic Fracturing Engineering[J]. *Chin. J. Rock Mech. Eng.* 36 (12), 2926–2939. doi:10.13722/j.cnki.jrme.2017.0405

Zeng, L., Gong, L., Guan, C., Zhang, B., Wang, Q., Zeng, Q., et al. (2022). Natural Fractures and Their Contribution to Tight Gas Conglomerate Reservoirs: A Case Study in the Northwestern Sichuan Basin, China. *J. Petroleum Sci. Eng.* Volume 210, 110028 pages. doi:10.1016/j.petrol.2021.110028

Zhenzhong, C., Hui, Z., Haijun, Y., Guoqing, Y, Yongfeng, Z, Peisi, C, et al. (2015). Investigation of Geomechanical Response of Fault in Carbonate Reservoir and its Application to Well Placement Optimization in YM2 Oilfield in Tarim Basin. In The SPE Annual Technical Conference and Exhibition held in Houston, Texas, USA, 28–30 September 2015. SPE-175017-MS.

Zoback, M. D., Kohli, A., Das, I., and Mcclure, M. (2012). The Importance of Slow Slip on Faults during Hydraulic Fracturing Stimulation of Shale Gas Reservoirs [C], In Society of Petroleum Engineers SPE Americas Unconventional Resources Conference, Pennsylvania, USA Pittsburg, 1–9. doi:10.2118/155476-MS

Zoback, M. D. (2007). *Reservoir Geomechanics*. Cambridge: Cambridge University Press.

Conflict of Interest: Authors GY, HZ, YX, WZ, XW, JL, and SL were employed by PetroChina Tarim Oilfield Company.

The remaining authors declare that the research was conducted in the absence of any commercial or financial relationships that could be construed as a potential conflict of interest.

Publisher's Note: All claims expressed in this article are solely those of the authors and do not necessarily represent those of their affiliated organizations, or those of the publisher, the editors, and the reviewers. Any product that may be evaluated in this article, or claim that may be made by its manufacturer, is not guaranteed or endorsed by the publisher.